A New Intelligent Hybrid Control Approach for DC–DC Converters in Zero-Emission Ferry Ships

Mohammad Hassan Khooban, *Senior Member, IEEE*, Meysam Gheisarnejad, Hamed Farsizadeh, Ali Masoudian, and Jalil Boudjadar, *Member, IEEE*

***Abstract*—Nowadays, sea traveling is increasing due to its practicality and low-cost. Ferry boats play a significant role in the marine tourism industry to transfer passengers and tourists. Nevertheless, traditional ferry ships consume massive amounts of fossil fuels to generate the required energy for their motors and demanded loads. Also, by consuming fossil fuels, ferries spatter the atmosphere with CO_2 emissions and detrimental particles. In order to address these issues, ferry-building industries try to utilize renewable energy sources (RESs) and energy storage systems (ESSs), instead of fossil fuels, to provide the required power in the ferry boats. In general, full-electric ferry (FEF) boats are a new concept to reduce the cost of fossil fuels and air emissions. Hence, FEF can be regarded as a kind of dc stand-alone microgrid with constant power loads (CPLs). This article proposes a new structure of a FEF ship based on RESs and ESSs. In order to solve the negative impedance induced instabilities in dc power electronic based RESs, a new intelligent single input interval type-2 fuzzy logic controller based on sliding mode control is proposed for the dc–dc converters feeding CLPs. The main feature of the suggested technique is that it is mode-free and regulates the plant without requiring the knowledge of converter dynamics. Finally, we conduct a dSPACE-based real-time experiment to examine the effectiveness of the proposed energy management system for FEF vessels.**

***Index Terms*—dc microgrid control, full-electric ferry, power electronic converters.**

I. Introduction

ONE of the most considerable contributors to the environmental issues (e.g., air emission, acid rain, greenhouse destructive effects) is marine power systems. In simpler terms, conventional marine power systems are mostly designed based on diesel generators, which operate by consuming fossil fuel [1]–[3]. Even though marine vessel emissions have not been considered in the Kyoto accord, stringent rules have been established by first world countries to reduce the emissions produced by marine power systems. On the other hand, the variation in fuel prices needed the motivation to explore more developed technology and proficient solutions to decrease operational costs in the marine tourism industry [4], [5]. In consequence, shipbuilding industries have tried to applied new advanced renewable energy sources (RESs) (e.g., fuel cell and photovoltaic) in the marine power system instead of using diesel generator systems.

The full-electric ferry (FEF) ships are presently of attention for boat commercial marine industries to build zero-emission and fuel-efficient operation. In this regard, there exist a few pieces of research about the zero-emission ferry. For instance, an emission-free sailboat is investigated in [6]. In this article, for required energy in the case study, the green energies, such as photovoltaics, eolic, and hydrogenation, are utilized. However, due to space limitations in the sailboat, applying these RESs together in a small ship is not feasible. A new intelligent energy management algorithm for hybrid electric ships is presented in [7]. In this work, the authors have used different RESs (e.g., wind turbine, solar panel, and fuel cell) for providing required power in the marine vessel. However, the feasibility of applying these various green energy units together is not assessed. The feasibility of applying fuel cell in the marine vessel system is investigated in [8]. In [9], a model predictive dc–dc converter control is proposed to reduce the pulse power loads effects in the marine power systems.

In typical cases, a marine vessel system with different renewable energy units and various energy storage systems (ESSs) can be regarded as a special dc stand-alone modern power grid with constant power loads [10], [11]. Fig. 1 shows the overall structure of a modern power grid with various RESs and loads. In this inverter-based dc modern islanded power grid, a robust and high-performance control approach is necessitated to reduce the negative impedance behavior. Hence, several works are proposed to address this difficulty in the stand-alone dc microgrid (MG) [12]–[16]. For instance, Vafamand *et al*. [12] present a model-based Takagi–Sugeno (TS) fuzzy system control for the stabilization of dc MGs under constant power loads (CPLs). In [13], a new method is introduced for controlling dc–dc converters that feed constant power loads. The control signal is achieved from feedback linearization, where the nonlinear transformation is a function of the power of an unknown load

Manuscript received June 9, 2019; revised September 3, 2019; accepted October 25, 2019. Date of publication November 3, 2019; date of current version February 20, 2020. This work was supported by the Energy Technology Development and Demonstration Program (EUDP) under Grant 64018-0721 (HFC: Hydrogen Fuel Cell and Battery Hybrid Technology for Marine Applications), Denmark. Recommended for publication by Associate Editor Prof. D. Maksimovic. *(Corresponding author: Mohammad Hassan Khooban.)*

M. H. Khooban and J. Boudjadar are with the Department of Engineering, Aarhus University, Åbogade 34, 8000 Aarhus, Denmark (e-mail: khooban@ieee.org; jalil@eng.au.dk).

M. Gheisarnejad is with the Department of Electrical Engineering, Najafabad Branch, Islamic Azad University, Isfahan 8514143131, Iran (e-mail: me.gheisarnejad@gmail.com).

H. Farsizadeh is with the Department of Electrical and Electronics Engineering, Shiraz University of Technology, Shiraz 71557-13876, Iran (e-mail: hthfarsi@gmail.com).

A. Masoudian is with the School of Electrical and Computer Engineering, Shiraz University, Shiraz, Iran (e-mail: a.masoudian@shirazu.ac.ir).

Color versions of one or more of the figures in this article are available online at http://ieeexplore.ieee.org.

Digital Object Identifier 10.1109/TPEL.2019.2951183

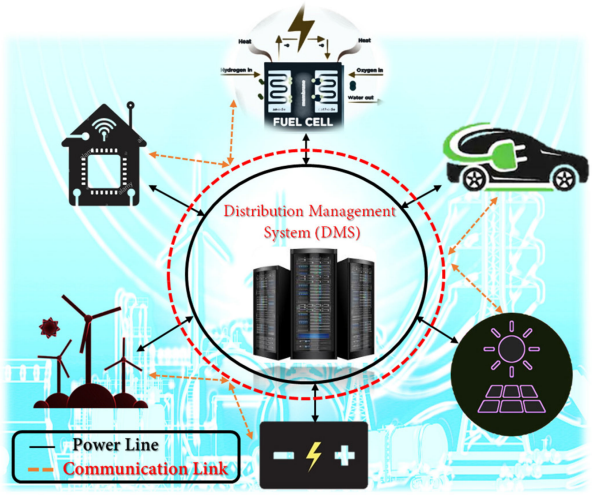

Fig. 1. General scheme of modern power grids.

and its time derivative. The work in [16] presents the use of a state-trajectory controller with embedded droop control in one of the source-end converters in order to improve three critical aspects of the MG operation: resiliency under large CPL's steps, load transient voltage regulation, and voltage transient recovery time. Nevertheless, most of these research works are based on the model-based control, such as model predictive control (MPC) [9] and sliding mode control (SMC) [17]. Conventional model-based approaches often develop with fine-grained knowledge of plant dynamics and their operational conditions. However, these approaches fail to ensure satisfactory results when there is no access to system modeling. Alternatively, model-free techniques (e.g., fuzzy logic control (FLC), etc. [18]) are mostly preferred in practice since they do not need the complexity of the system dynamic identification.

Recently, a new model-free technique based on the intelligent proportional-integral-derivative (iPID) controller and its variants was implemented successfully in the real-time systems, like vehicle control [19], robotic [20], dc–dc converters [18], etc. The design procedure of this control technique mainly relies on the input-output (I/O) measured information of the plant; therefore, there is no need to identify the system models as it utilizes an observer based on algebraic schemes to approximate the unknown dynamics. Due to the measurement noises, this algebraic technique is not able to guarantee the path tracking error to converge to zero quickly. To overcome this problem, an extended state observer (ESO) is often embedded in the model-free control structure to estimate the unknown dynamics [21]. Effective model-free control can be guaranteed by setting the ESO coefficient properly and bounding the unknown dynamics. Perversely, a non-zero estimate error always appears when the observer is not set up well. An input compensator, such as fuzzy logic, SMC, and neural network, can be a possible solution for the elimination of ESO estimation errors and it can be integrated into the iPID controller [22], [23].

This article focuses on utilizing fuel cells (FCs) as the main source of the required energy for the demanded loads. Therefore, in the first step, a new structure of the hybrid fuel cell/battery-based ferry ship is presented. The whole of the system under study is considered as an islanded dc MG with constant power loads. One of the main challenges in dc MG is to decrease the negative impedance instability. Thus, a novel intelligent single input interval type-2 fuzzy PI controller (iSIT2-FPI) based on SMC is proposed to stabilize the dc–dc boost converter connected to CPLs. The suggested control technique combines the SMC and the model-free iSIT2-FPI control to compensate the destructive impedance instabilities. The proposed method is easy to design as well as it does not need the mathematical model of the system. In simpler terms, by having only some input/output signals, the dc–dc converter can be controlled accurately. Finally, we conduct a dSPACE-based real-time experiment to examine the effectiveness of our method for the dc–dc converter control in FEF vessels.

II. Stand-Alone DC Ferry Microgrid Model

In this article, instead of using diesel generator engines to provide the power to the ferry boat, FCs are utilized. Due to the slow dynamic response of FCs, batteries are utilized to compensate for this issue [24]. ESSs are mainly utilized to provide the high dynamic part of the loads that FCs cannot supply. In addition, another application of batteries in all-electric-ferry is to enable FCs to operate in their optimal efficiency. In Fig. 2, the overall structure of the FEF boat is illustrated.

It can be seen from Fig. 2 that the structure of the proposed hybrid FC/Battery can be assumed to be a dc islanded MG with CPLs. In simpler terms, various loads, such as motor drives or electronic loads, with tightly regulated controllers behave as a constant power load [25]. The main focus of this article is to introduce a high-performance and fast controller for the dc–dc converter feeding CPLs to decrease the negative impedance instability in the ferry power grid.

The diagram of a dc–dc boost converter feeding a CPL in DC MG is depicted in Fig. 2. The green power unit (e.g., FC, PV, or wind turbine) is connected to the main dc link to supply the CPL (e.g., motors or other loads). E shows the fuel cell output power and the overall demanded load is introduced by a CPL, which shows a worst scenario condition from the stability point of view.

Normally, in the modern dc power grid, the stabilization of the dc link voltage and supplying the CPL is conducted by dc–dc converters [17]. To design controllers for this kind of converters, the state-space averaged model is used. Hence, the mathematical model of a typical dc–dc converter can be expressed as [26]:

$$\frac{di_L}{dt} = \frac{E}{L} - \frac{(1-u)}{L} v_C \tag{1}$$

$$\frac{dv_C}{dt} = \frac{(1-u)}{C} i_L - \frac{P}{Cv_C} \tag{2}$$

where i_L and v_C are the average of the inductor current and capacitor voltage, respectively. L and C are the inductance and capacitance of the dc–dc boost converter, respectively. Moreover, $u \in \{0, 1\}$, is the control input. In practice, i_L and v_C are limited parameters; therefore, it is necessary to constrain the

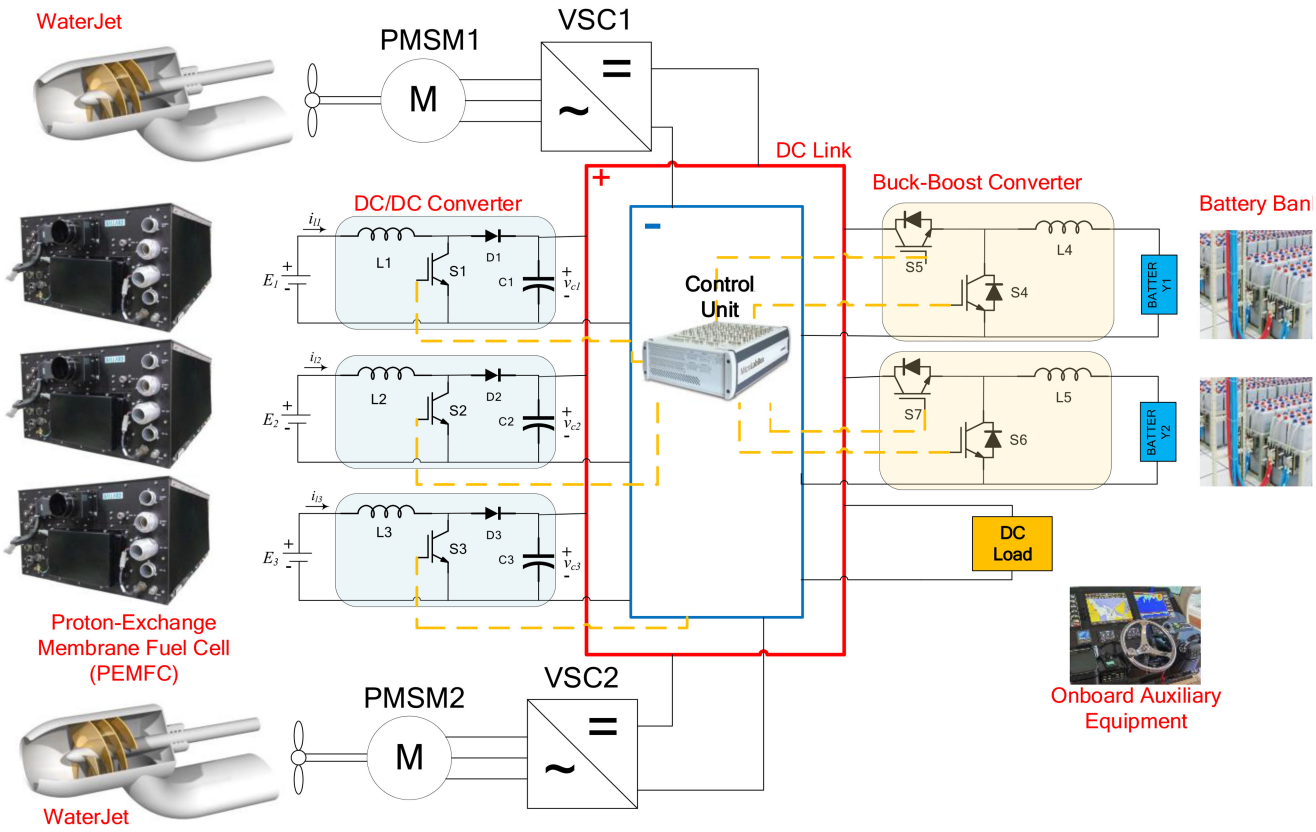

Fig. 2. Overall scheme of the stand-alone dc ferry grid.

values of i_L and v_C. Furthermore, i_L and $v_C \in \phi$, where ϕ is a subset of R^2, i.e.

$$i_L, v_C \in \phi \subseteq R^2 \backslash \{0\}. \tag{3}$$

The readers can refer to [26] and [27] in order to acquire more information about the mathematical modeling of dc–dc converters. Conventionally, the PID controller and its variants are one of the most famous and useful classic controllers, which are applied in a wide variety of power electronic applications. However, since the performance of these kinds of controllers depends on an operation point, they cannot have the desired performance when the operation point of the system changes. In order to address this issue, this article introduces a new intelligent controller for dc–dc converters to have a fast and efficient response.

III. Controller Design

In this section, a novel model-free control strategy, which is made of three sub-components, is designed and integrated into the concerned FEF. Initially, ESO is adopted to estimate the process of uncertain data by the knowledge of its control input–output parameters. Then, a model-free based iSIT2-FLC is established to reduce the complexity of the existing controller, enter required control specifications, and suppress the high-order derivative output. The SMC is implemented to eliminate the ESO estimation error.

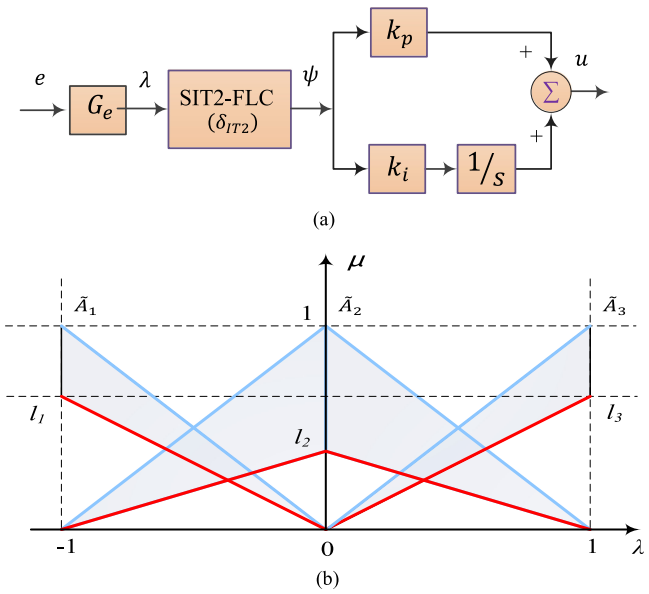

Fig. 3. Schematic diagram of (a) SIT2-FPI structure and (b) triangular MFs.

A. PI-Type SIT2-FLC

1) Basic Structure of the Interface Mapping IT2-FPI: In Fig. 3(a), the general form of one-to-one inference mapping SIT2-FPI controller is illustrated. In the structure, the error

signal is normalizied by the scaling factor (SF) G_e. Thus, the error signal (e) is converted into λ, which is the input coefficient of the SIT2-FPI structure. A simple normalization ensures that λ will be within the universe of discourse $[-1, +1]$. The output of the configured SIT2-FPI controller ψ, depicted in Fig. 3(a), is transformed into a control signal (u) as follows:

$$u(t) = k_p\ \psi + k_i \int \psi \tag{4}$$

where

$$k_p = k_{p0}\ \ G_u; k_i = k_{i0}\ G_u.$$

Here, k_{p0} and k_{i0} denote the baseline PI controller coefficients and G_u denotes the output SF, which is defined as $G_u = G_e^{-1}$.

2) SIT2-FLC Design Scheme: The rule structure of each SIT2-FLC is expressed as [3], [28]

$$r_i: \text{ if } e \text{ is } \tilde{A}_i \text{ then } e_{\mathrm{IT2}} \text{ is } B_i, i = 1, 2, 3. \tag{5}$$

The antecedent membership functions (MFs) are made by a triangular type of IT2 fuzzy sets (IT2FSs) $\tilde{A}_i$, as depicted in Fig. 3(b). The crisp consequents B_i are generated by the following values: $B_1 = -1$, $B_2 = 0$, and $B_3 = 1$. IT2FSs can be defined based on the lower MF ($\underline{\mu}_{\tilde{A}_n}$) and upper MF ($\overline{\mu}_{\tilde{A}_n}$). In Fig. 3(b), l_i ($i = 1$, 2, and 3) is the height of the lower MFs. In this article, the symmetrical MFs are adopted with the following assumptions: $l_1 = l_3 = 1 - \delta_{\mathrm{IT2}}$ and $l_2 = \delta_{\mathrm{IT2}}$. Here, δ_{IT2} is the main SIT2-FPI coefficient, which should be adjusted with respect to the required system performance.

By using the center of set-type reduction scheme [28], the output of IT2-FLC is defuzzified as$\varphi_o = (\varphi_o^r + \varphi_o^l)/2$, where φ_o^r and φ_o^l are the end points of the type reduced set and obtained by

$$\varphi_o^l = \frac{\sum_{n=1}^{L} \overline{\mu}_{\tilde{A}_n}(\lambda)\,.\,B_n + \sum_{n=L+1}^{N} \underline{\mu}_{\tilde{A}_n}(\lambda)\,.\,B_n}{\sum_{n=1}^{L} \overline{\mu}_{\tilde{A}_n}(\lambda) + \sum_{n=L+1}^{N} \underline{\mu}_{\tilde{A}_n}(\lambda)} \tag{6}$$

$$\varphi_o^r = \frac{\sum_{n=1}^{R} \underline{\mu}_{\tilde{A}_n}(\lambda)\,.\,B_n + \sum_{n=R+1}^{N} \overline{\mu}_{\tilde{A}_n}(\lambda)\,.\,B_n}{\sum_{n=1}^{R} \underline{\mu}_{\tilde{A}_n}(\lambda) + \sum_{n=R+1}^{N} \overline{\mu}_{\tilde{A}_n}(\lambda)}. \tag{7}$$

Here, *L* and *R* denote the switching points.

Based on [29] and [30], the fuzzy mappings (FM) of SIT2-FLC can be described as

$$\psi\ (\lambda) = \lambda.\ k\,(|\lambda|) \tag{8}$$

where $k(\lambda)$ is a nonlinear coefficient derived from SIT2-FLC and is expressed as

$$k\ (\lambda) = \frac{1}{2}\ \left(\frac{1}{\delta_{\mathrm{IT2}} + \lambda - \delta_{\mathrm{IT2}}\lambda} + \frac{\delta_{\mathrm{IT2}} - 1}{\delta_{\mathrm{IT2}}\lambda - 1}\right). \tag{9}$$

Defining $\varepsilon_o(\lambda) = \psi(\lambda) - \lambda$, the three mapping IT2-FLC modes based on the control curve (CC) can be obtained for various constraints of δ_{IT2}, as described in Table I. In Fig. 4, examples of A-$\mathrm{CC_{IT2}}$, S-$\mathrm{CC_{IT2}}$, and M-$\mathrm{CC_{IT2}}$ are presented for $\delta_{\mathrm{IT2}} = 0.2$, $\delta_{\mathrm{IT2}} = 0.4$, $\delta_{\mathrm{IT2}} = 0.5$, $\delta_{\mathrm{IT2}} = 0.6$, and $\delta_{\mathrm{IT2}} = 0.8$. For more details about the CCs generations of the SIT2-FLC, the readers are referred to Sarabakha *et al.* [28].

To preserve the features of both A-$\mathrm{CC_{IT2}}$ and S-$\mathrm{CC_{IT2}}$, the footprint of uncertainty (FOU) coefficient of SIT2-FPI is set to 0.5 to generate M-$\mathrm{CC_{IT2}}$ mode. Since the maximum error is less than 1, the input and output SFs are set to 1.

TABLE I
DEFINITIONS OF SIT2-FLC UNDER DIFFERENT CONSTRAINTS OF δ_{IT2}

	Design Variables	Type of CC
Mode-1	If $0 < \delta_{IT2} \le \delta_{c1}$, then $\varepsilon > 0$ for $\forall\,\lambda \in [0, 1)$ and $\delta_{c1} = (3 - \sqrt{5})/2$	Aggressive $\mathrm{CC_{IT2}}$ (A-$\mathrm{CC_{IT2}}$)
Mode-2	If $\delta_{c2} \le \delta_{IT2} < 1$, then $\varepsilon < 0$ for $\forall\,\lambda \in [0, 1)$ and $\delta_{c2} = (\sqrt{5} - 1)/2$	Smooth $\mathrm{CC_{IT2}}$ (S-$\mathrm{CC_{IT2}}$)
Mode-3	If $\delta_{c1} < \delta_{IT2} < \delta_{c2}$, then $\varepsilon > 0$ for $\forall\,\lambda \in [0, 0.5)$ and $\varepsilon < 0$ for $\forall\,\lambda \in [0.5, 1)$	Moderate $\mathrm{CC_{IT2}}$ (M-$\mathrm{CC_{IT2}}$)

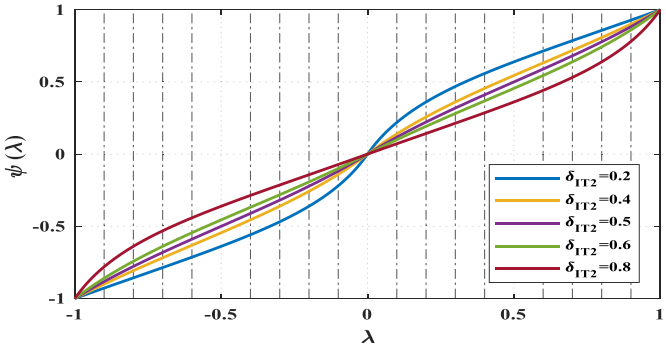

Fig. 4. Illustration of the control surfaces with different values of δ_{IT2}.

B. Intelligent PI-Type SIT2-FLC-Based Sliding Mode Control

1) Proposed intelligent PI-type SIT2-FLC: For a general single-input single-output (SISO) nonlinear plant, the model-free scheme is characterized based on an ultra-local model as follows [21], [31]:

$$y^{(v)}(t) = \Phi + \Lambda u(t) \tag{10}$$

where $y^{(v)}(t)$ is the derivative of order $v \in \mathbb{N}$ of the output $y(t)$, which is usually in practice chosen as 1 or 2. Φ denotes an unknown term, which is identified by the control signal $u(t)$ and output $y(t)$. $\Lambda \in \mathbb{R}$ is a nonphysical design constant, which is selected so that $\Lambda u(t)$ and $y^{(v)}(t)$ have the same order of magnitude.

Remark 1: Note that the order of differentiation v does not have any relation to the unknown plant and may, in general, be selected quite small, i.e., 1, 2. In almost all available concrete research works, $v = 1$, while only a few case-studies are provided by $v = 2$ [32].

Remark 2: Φ will be constantly updated during the simulation. This term reflects the unknown parts of the system dynamics as well as the different possible disturbances. The ESO (see, e.g., [23], [33], and the references therein) is used to estimate the coefficient $\hat{\Phi}$ and feed back to the iSIT2-FPISMC structure. The iSIT2-FPISMC technique can be adopted to design the dc–dc boost converter controller without requiring the specific model of the stand-alone dc ferry MG.

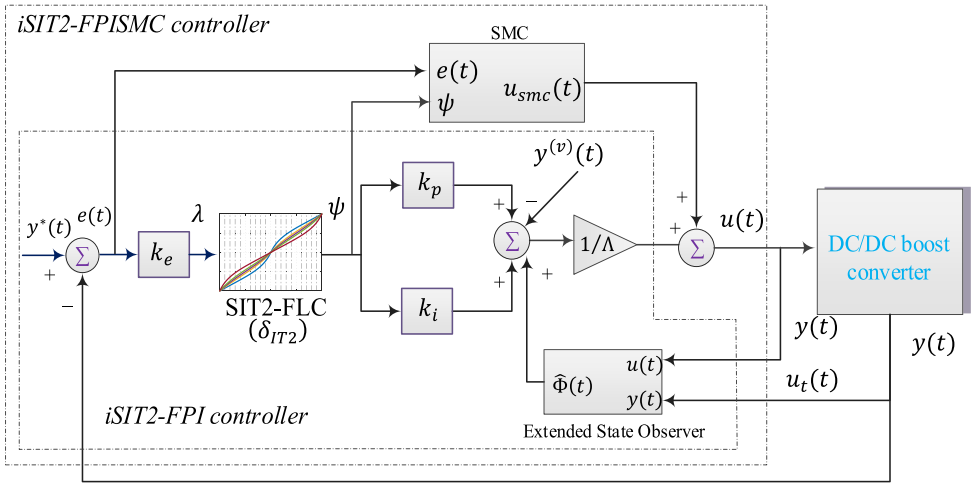

Fig. 5. Schematic diagram of the iSIT2-FPISMC.

If Φ and Λ are well-known items, an iSIT2-FPI can be suggested as

$$u\ (t) = \frac{1}{\Lambda}\left(-\hat{\Phi}\,(t) + \ y^{(v)^*} + k_p\psi_u + k_i\int\psi_u\right) \tag{11}$$

where $y^{(v)^*}$ is the output desired reference with the derivative of order v and $\hat{\Phi}(t)$ is the estimated value of $\Phi(t)$. Combining (10) and (11), the error equation $e^{(v)}\ (t) = y^{(v)^*}\,(t) - y^{(v)}(t)$ is obtained as

$$e^{(v)}\,(t) + \Phi - \hat{\Phi} + k_p\psi_u + k_i\ \int\psi_u = \ 0. \tag{12}$$

The estimated disturbance $\hat{\Phi}$ in this article will be calculated by employing ESO. ESO is designed by a third observer as [20], [28]

$$\begin{aligned}\dot{q}_1 &= q_2 - \mu_{o1}\mathrm{fal}\,(F,\omega_1,\ \rho)\\ \dot{q}_2 &= q_3 - \mu_{o2}\mathrm{fal}\,(F,\omega_2,\ \rho)\\ \dot{q}_3 &= -\mu_{o3}\mathrm{fal}\,(F,\omega_3,\ \rho)\end{aligned} \tag{13}$$

where μ_{o1}, μ_{o2}, and μ_{o3} represent the observer constant, q_1, q_2, and q_3 represent the intermediate states and F is the estimated error of observer. In the ESO scheme, q_3 denotes the estimation generated by the observer; therefore, we have $q_3 = \hat{\Phi}$.

$$\mathrm{fal}\ (F,\omega,\ \rho) = \begin{cases}|F|^{\omega}\mathrm{sgn}\,(F)\,,\ |F| > \rho\\ F/\rho^{1-\omega},\ \text{otherwise}\end{cases} \tag{14}$$

where $0 \le \omega \le 1$ and $\rho > 0$.

2) Design of a Model-Free Sliding Mode Control: According to (11), the quality of iSIT2FPI actions depends on the baseline PI gains of SIT2-FLC, FOU design coefficient, and estimation of Φ. An inaccurate estimation with large error leads to degrading the performance of the mode-free technique. To remove the estimation error, an additional controller SMC is provided. The overall structure of the hybrid iSIT2FPI, and SMC is highlighted in Fig. 5. The extra SMC input control is represented by u_{smc} and it results in

$$u\ (t) = \frac{1}{\Lambda}\left(-\hat{\Phi}\,(t) + \ y^{(v)^*} + k_p\psi_u + k_i\int\psi_u\right) + u_{\mathrm{smc}}. \tag{15}$$

Let the estimated error of observer be defined as $\tilde{\Phi} = \Phi - \hat{\Phi}$. Based on [23], one has $\tilde{\Phi} < \Phi_m$, where Φ_m is an upper bound. Substituting (15) into (10), the error equation with the order of $v = 2$ is yielded as

$$\ddot{e}\,(t) + k_p\psi_u + k_i\int\psi_u + \Lambda u_{\mathrm{smc}} + \tilde{\Phi}\ \ (t) = 0. \tag{16}$$

According to the SMC design scheme, a switching function is introduced as

$$\sigma = \gamma e\,(t) + \dot{e}\,(t) \tag{17}$$

where $\gamma > 0$ is a design coefficient. The derivative of (17) is calculated as

$$\begin{aligned}\dot{\sigma}\ \ (t) = \gamma\dot{e}\,(t) + \ddot{e}\ \ (t) &= \gamma\dot{e}\,(t) - k_p\psi_u - k_i\int\psi_u\\ &\quad - \Lambda u_{\mathrm{smc}} - \tilde{\Phi}\,(t)\,.\end{aligned} \tag{18}$$

The extra input u_{smc}, which consists of equivalent control u_{eq} and switching control u_{sw}, is defined as $u_{\mathrm{smc}} = u_{\mathrm{eq}} + u_{\mathrm{sw}}$. In order to reach the desired sliding mode condition in (18), u_{eq} is obtained by replacing $\tilde{\Phi}$ with Φ_m as

$$u_{\mathrm{eq}} = \frac{1}{\Lambda}\ \left(\gamma\dot{e}\,(t) - k_p\psi_u - k_i\int\psi_u - \Phi_m\right). \tag{19}$$

In order to eliminate the chattering effects, u_{sw} is defined as

$$u_{\mathrm{sw}} = \frac{1}{\Lambda}\ \left(\eta_1\left[\mathrm{sat}\,(\sigma,\varepsilon)\right] + \eta_2\sigma\right). \tag{20}$$

where η_1 and η_2 denote the switching gains, ε denotes the boundary thickness, $\eta_1 > 0$, $\eta_2 > 0$, and $\varepsilon > 0$, and

$$\mathrm{sat}\,(\sigma,\varepsilon) = \begin{cases}1 & \text{if}\,\sigma > \varepsilon\\ \sigma/\varepsilon & \text{if}\ \ |\sigma| \le \varepsilon\\ -1 & \text{if}\,\sigma < -\varepsilon\end{cases}. \tag{21}$$

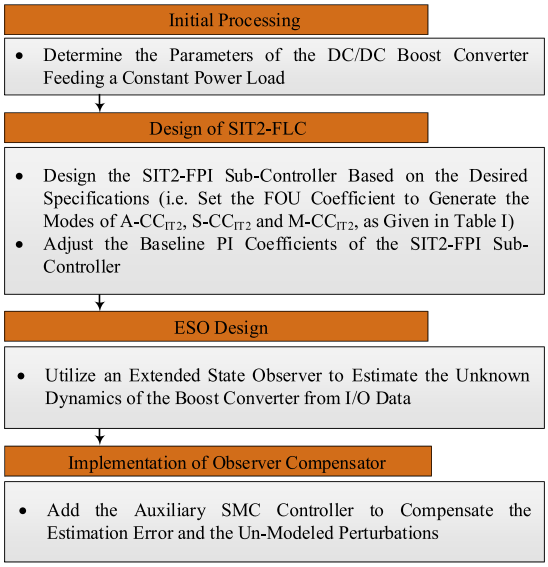

Fig. 6. Design steps of the proposed framework.

Substituting the extra input u_{smc} into (15), the total control signal can be rewritten as

$$u(t) = \frac{1}{\Lambda}\left(-\Phi_m - \hat{\Phi}(t) + y^{(v)*} + \eta_1 \left[\text{sat}(\sigma(t), \varepsilon)\right] + \eta_2\sigma + \gamma\dot{e}(t)\right). \quad (22)$$

3) Stability Analysis: Consider the Lyapunov function as

$$V = \frac{1}{2}\sigma^2. \quad (23)$$

The derivative of (23) yields

$$\dot{V} = \sigma\,\dot{\sigma} = -\sigma\left(\eta_1\left[\text{sat}(\sigma, \varepsilon)\right] + \tilde{\Phi} - \Phi_m\right) - \eta_2\sigma^2. \quad (24)$$

Therefore, the boundedness of $\tilde{\Phi}$ is sufficient to satisfy $\dot{V} < 0$. For $|\sigma| < \varepsilon$ and $|\sigma| > \varepsilon$, Lyapunov stability can be assured under two situations [34]:

Case 1: If $|\sigma| > \varepsilon$, the existing condition will be converted as

$$\dot{V} = -\sigma\left(\eta_1 + \tilde{\Phi} - \Phi_m\right) - \eta_2\sigma^2. \quad (25)$$

According to the boundedness of $\tilde{\Phi}$, it is met that $\dot{V} < 0$ if one has $\eta_1 > 2\Phi_m$.

Case 2: If $|\sigma| < \varepsilon$, the existing condition will be changed as

$$\dot{V} = -\sigma\left(\eta_1\sigma/\varepsilon + \tilde{\Phi} - \Phi_m\right) - \eta_2\sigma^2. \quad (26)$$

Defining the condition of (26), the negative term on the right-hand side is met

$$-\sigma\left(\tilde{\Phi} - \Phi_m\right) - (\eta_1/\varepsilon + \eta_2)\sigma^2 < 0.$$

$$\left|\tilde{\Phi} - \Phi_m\right| < (\eta_1/\varepsilon + \eta_2)\sigma \quad (27)$$

Considering the boundedness of $\tilde{\Phi}$ and $|\sigma| < \varepsilon$, one can get $(\eta_1 + \varepsilon\eta_2) > 2\Phi_m$.

The flowchart of the proposed framework is sketched in Fig. 6.

TABLE II
THE CASE-STUDY PARAMETERS

Parameter	Value
L	1 mH
C	1000 μf
E	48 V
V_{ref}	110 V
P	500 W

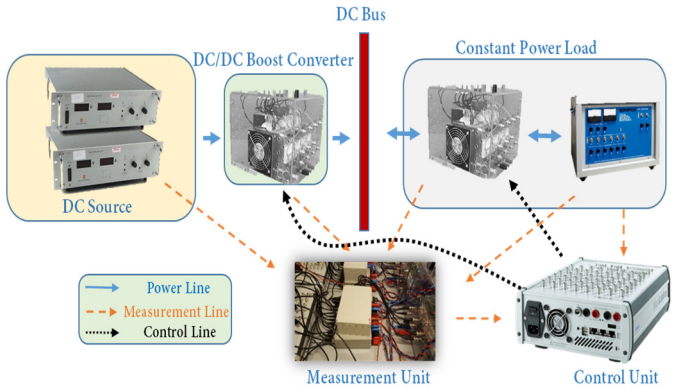

Fig. 7. Real-time setup and configuration of the marine dc MG benchmark.

IV. EXPERIMENTAL RESULTS

In this section, hardware-in-the loop (Hil) real-time simulation on a dc–dc boost converter with one dc power supply and one constant power load is done to demonstrate the applicability of the suggested technique. Additionally, the parameters of the dc–dc boost converter are stated in Table II. Fig. 7 presents the overall structure of the experimental setup. The novel control method is applied in a dSPACE MicroLabBox with DS1202 Power PC Dual-Core 2-GHz processor board and DS1302 I/O board with the sampling time 100 μs.

In this article, a novel intelligent SIT2-FPI-based SMC has been developed for a boost converter supplying a CPL in a stand-alone dc ferry MG. The Hil simulation is carried out for the CPL voltage reference $V_{\text{ref}} = 110[V]$. Furthermore, to show the performance improvement of the proposed approach, the iPI [31] and MPC [35] is developed for the case of this article. Figs. 8–10 show the tracking power of the CPL, voltage of the DC bus, and the current of the inductor, respectively, for the proposed approach and other controllers [7].

A. Scenario 1: Constant Power Load Variations

In order to make a good challenge for the proposed control method, the CPL power is assumed to change over time. In this scenario, the CPL power with the operating condition of $P = 500$ [w] is decreased to 300 $[w]$ at $t = 0.3$ s and is also increased to 700 $[w]$ at $t = 0.7$ s. From the experimental results, it is simply found that by adopting the proposed method, the voltage response maintains a constant value, while the inductor current references are tracked precisely. As can be seen in Figs. 8–10, the proposed approach leads to a higher level

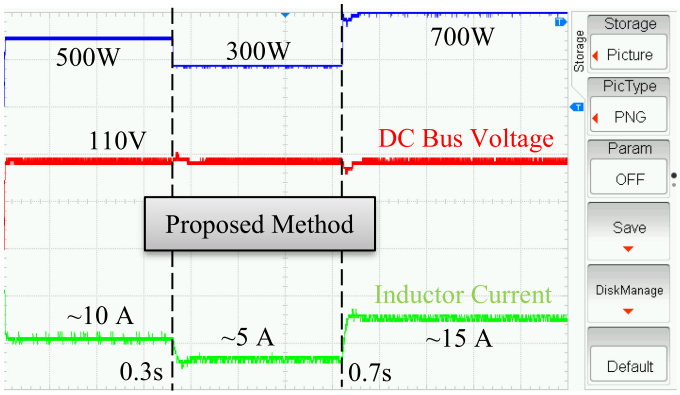

Fig. 8. Transient performance of the iSIT2-FPISMC controller (the CPL power changes, dc bus voltage, and inductor current are shown with blue, red, and green curves, respectively).

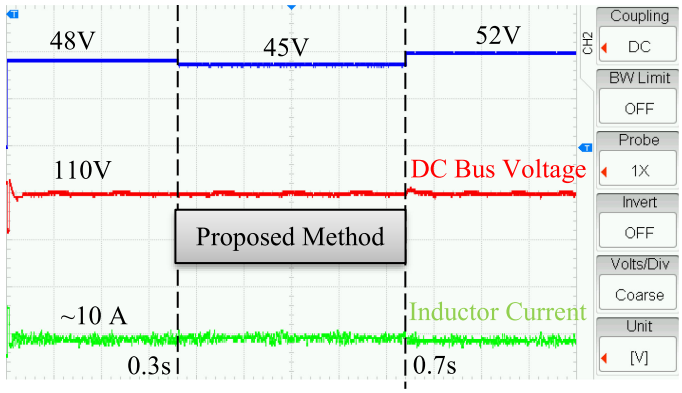

Fig. 11. Input voltage variations of the converter—the iSIT2-FPISMC controller (the input voltage changes, dc bus voltage, and inductor current are shown with blue, red, and green curves, respectively).

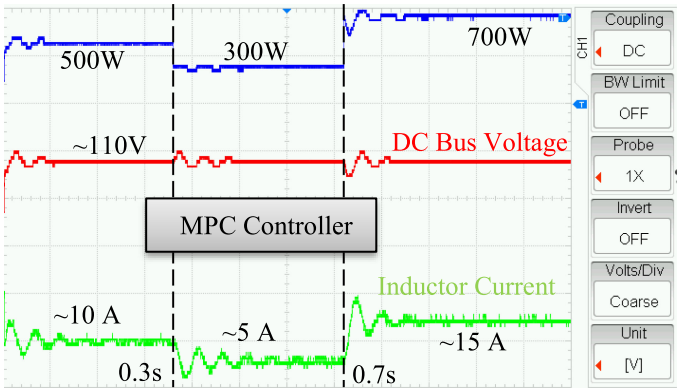

Fig. 9. Transient performance of the MPC controller (the CPL power changes, dc bus voltage, and inductor current are shown with blue, red, and green curves, respectively).

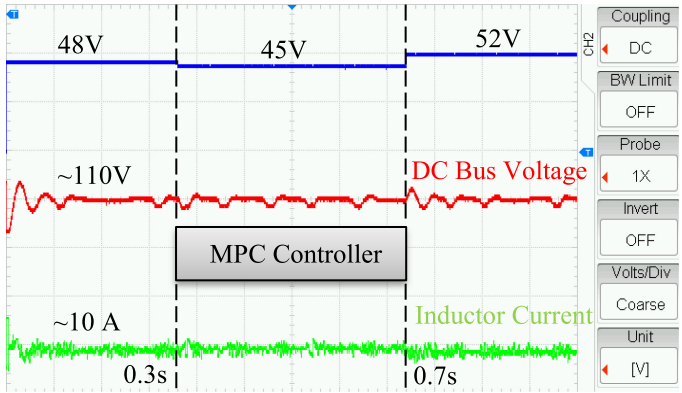

Fig. 12. Input voltage variations of the converter—the MPC controller (the input voltage changes, dc bus voltage, and inductor current are shown with blue, red, and green curves, respectively).

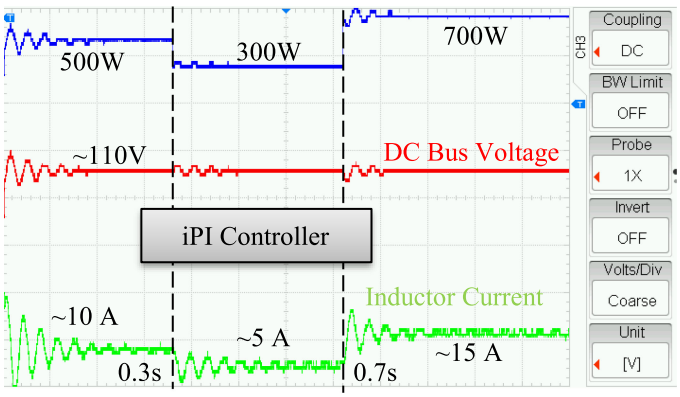

Fig. 10. Transient performance of the iPI controller (the CPL power changes, dc bus voltage, and inductor current are shown with blue, red, and green curves, respectively).

of reliable operation of the marine MG against the uncertain time-varying loads than the iPI and MPC controllers.

The reason is that the MG responses with the proposed method experience fewer fluctuations than the state-of-the-art methods, and therefore they are more desirable from the engineering power point of view. It can be concluded that the proposed model-free method guarantees the supply of constant power required by the load and is robust with reference to the time-varying loads.

B. Scenario 2: Input Voltage Variations

In this case, the step-up change in the converter's reference voltage aims to validate the controller's real-time reference tracking ability. In order to validate the performance and robustness of the proposed method over input voltage variations, the converter's reference voltage is changed from 48 V at 0.3 s to 45 V, and also changed from 45 V at 0.7 to 52 V. Figs. 11–13 illustrate the experimental results.

As shown in Figs. 11–13, the iSIT2-FPISMC controller has a better performance over other control techniques to stabilize the dc bus voltage as well as it is superior to damp the voltage oscillations.

V. Discussion

The negative impedance feature of CPLs strongly threatens the stability of the entire dc shipboard MG plant. Despite the

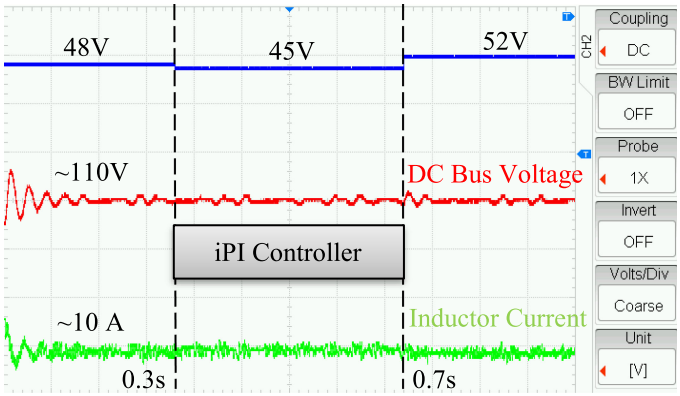

Fig. 13. Input voltage variations of the converter—the iPI controller (the input voltage changes, dc bus voltage, and inductor current are shown with blue, red, and green curves, respectively).

rich body of literature in the context of dc shipboard MGs with CPLs, majority of the existing studies considered that the controller can be adopted without any uncertainties, and the value of plant parameters is precisely identified. However, in practice, we are faced with an unstructured environment; thus, the classic deterministic methodologies no longer can ensure the stability the dc shipboard MGs against the inaccuracies in the ESS models, quantization impacts, and computational controller delays. The above-mentioned specifications necessitate more robust strategies and more appropriate control tools for control synthesis challenges in the modern power MGs.

In response to the real-time marine MG situations, this article addresses an intelligent SIT2-FPI based on SMC to stabilize the dc MGs with time-varying CPLs. The main outcomes can be stated as follows:

1) The suggested control technique employs an intelligent SIT2-FPI-based ESO for the essential framework to enjoy its interesting model-free benefit, while the SMC part is applied to compensate the observer estimation errors. The suggested control actions are generated based only on the dc *shipboard* MG input/output signals. Under this framework, the suggested method can be implemented for reasonably wide forms of dc MGs with various configurations.
2) An effective structure of FC/battery in the FEF ships, which feeds a time-varying load, is investigated. It is demonstrated that the unknown dynamic part and the disturbances in a typical dc MG can be estimated by an observer, and this study opens the way to employ this article as a reference for more research studies in the context of robust MGs control.
3) The validation of the iSIT2-FPISMC controller is conducted by a real-time platform based on the model-in-the loop testbed in a real marine dc MG. The experimental outcome confirms the fluctuation reduction of the suggested method in comparison with the state-of-the-art approaches when the controller and the plant face the inaccuracies.
4) The minimal pollutant emissions of FCs (ideally only water for hydrogen fuel) make this technology attractive for power generation in the future ferry ships. Therefore, the concerns about the hazardous CO_2 emissions and oil consumption can be responded.
5) In the end, simultaneously considering time-varying CPLs, different power oscillations and inaccuracies in the dc marine MG problem among a control formulation via a model-free scheme can also be regarded as a remarkable outcome of this work.

VI. Conclusion

The propulsion of ships pollutes through the emission of CO_2 and harmful particles when operated by diesel engines. Electrification of ship propulsion is a way to introduce clean tech-solutions in the transport sector of special interests in harbors and costal zones. This article addresses the hybrid electrical propulsion of ships where the electrical power is partly supplied from batteries and partly generated on-board by means of FCs fueled by hydrogen. The process of generating electrical power from hydrogen is environmental-friendly as the exhaust is only water. The fuel cell technology will allow for faster refueling and longer distance between refueling compared to ships with only batteries. The hybrid combination of batteries and FCs will deliver efficient and reliable supply of electricity for propulsion. The goal of this article was to stabilize a special dc marine MG that has uncertain time-varying constant power loads and drive the dc voltage of the bus to track the desired voltage. To this aim, the model-free iSIT2-FPISMC was adopted to compensate the destructive impedance induced instabilities in the dc power electronic. Based on the concept of the ultra-local model, the suggested controller combines SMC scheme with the model-free iSIT2-FPI, constructing a new control structure. A comparison with MPC and iPI was conducted in the Hil real-time setup. The comparative real-time outcomes revealed that the suggested intelligent mode-free controller stabilizes the investigated test system much quicker than the other considered controllers. For future works, we aim to apply the novel proposed control technique to other power electronic devices (e.g., voltage source converter, bidirectional buck-boost converter, etc.) and compare the results to the prevalent proposed controllers, such as MPC, and fuzzy logic system. Moreover, in this article, we applied our proposed method only on one source and one CPL. Hence, in the next step, we will implement the suggested controller on completed ferry power gird with multi-power sources and CPLs, as shown in Fig. 2.

Acknowledgments

The authors would like to thank the reviewers who provided constructive comments that helped to improve the quality of this article. The authors are particularly grateful to the Editor-In-Chief and the Associate Editor for their constructive involvement and collaboration during few critical points of the review process. The publication of this paper would not have been possible, otherwise.

REFERENCES

[1] J. Han, J.-F. Charpentier, and T. Tang, "An energy management system of a fuel cell/battery hybrid boat," *Energies*, vol. 7, no. 5, pp. 2799–2820, Apr. 2014.

[2] M.-H. Khooban, T. Dragicevic, F. Blaabjerg, and M. Delimar, "Shipboard microgrids: A novel approach to load frequency control," *IEEE Trans. Sustain. Energy*, vol. 9, no. 2, pp. 843–852, Apr. 2018.

[3] R. Heydari, M. Gheisarnejad, M. H. Khooban, T. Dragicevic, and F. Blaabjerg, "Robust and fast voltage-source-converter (VSC) control for naval shipboard microgrids," *IEEE Trans. Power Electron.*, vol. 34, no. 9, pp. 8299–8303, Sep. 2019.

[4] S. Yousefizadeh, J. D. Bendtsen, N. Vafamand, M. H. Khooban, F. Blaabjerg, and T. Dragicevic, "Tracking control for a DC microgrid feeding uncertain loads in more electric aircraft: Adaptive backstepping approach," *IEEE Trans. Ind. Electron.*, vol. 66, no. 7, pp. 5644–5652, Jul. 2019.

[5] C. H. Choi *et al.*, "Development and demonstration of PEM fuel-cell-battery hybrid system for propulsion of tourist boat," *Int. J. Hydrogen Energy*, vol. 41, no. 5, pp. 3591–3599, Feb. 2016.

[6] L. K. C. Tse, S. Wilkins, N. McGlashan, B. Urban, and R. Martinez-Botas, "Solid oxide fuel cell/gas turbine trigeneration system for marine applications," *J. Power Sources*, vol. 196, no. 6, pp. 3149–3162, Mar. 2011.

[7] R. Ashok and Y. Shtessel, "Control of fuel cell-based electric power system using adaptive sliding mode control and observation techniques," *J. Franklin Inst.*, vol. 352, no. 11, pp. 4911–4934, Nov. 2015.

[8] F. Li, Y. Yuan, X. Yan, R. Malekian, and Z. Li, "A study on a numerical simulation of the leakage and diffusion of hydrogen in a fuel cell ship," *Renewable Sustain. Energy Rev.*, vol. 97, pp. 177–185, Dec. 2018.

[9] M. M. Mardani, M. H. Khooban, A. Masoudian, and T. Dragicevic, "Model predictive control of DC–DC converters to mitigate the effects of pulsed power loads in naval DC microgrids," *IEEE Trans. Ind. Electron.*, vol. 66, no. 7, pp. 5676–5685, Jul. 2019.

[10] N. Vafamand, M. H. Khooban, T. Dragicevic, and F. Blaabjerg, "Networked fuzzy predictive control of power buffers for dynamic stabilization of DC microgrids," *IEEE Trans. Ind. Electron.*, vol. 66, no. 2, pp. 1356–1362, Feb. 2019.

[11] N. Vafamand, S. Yousefizadeh, M. H. Khooban, J. D. Bendtsen, and T. Dragicevic, "Adaptive TS fuzzy-based MPC for DC microgrids with dynamic CPLs: Nonlinear power observer approach," *IEEE Syst. J.*, vol. 13, no. 3, pp. 3203–3210, Sep. 2019.

[12] N. Vafamand, M. H. Khooban, T. Dragicevic, F. Blaabjerg, and J. Boudjadar, "Robust non-fragile fuzzy control of uncertain DC microgrids feeding constant power loads," *IEEE Trans. Power Electron.*, vol. 34, no. 11, pp. 11300–11308, Nov. 2019.

[13] J. A. Solsona, S. G. Jorge, and C. A. Busada, "Nonlinear control of a buck converter which feeds a constant power load," *IEEE Trans. Power Electron.*, vol. 30, no. 12, pp. 7193–7201, Dec. 2015.

[14] S. Arora, P. Balsara, and D. Bhatia, "Input–output linearization of a boost converter with mixed load (constant voltage load and constant power load)," *IEEE Trans. Power Electron.*, vol. 34, no. 1, pp. 815–825, Jan. 2019.

[15] B. A. Martinez-Trevino, A. El Aroudi, A. Cid-Pastor, and L. Martinez-Salamero, "Nonlinear control for output voltage regulation of a boost converter with a constant power load," *IEEE Trans. Power Electron.*, vol. 34, no. 11, pp. 10381–10385, Nov. 2019.

[16] M. A. Bianchi, I. G. Zurbriggen, F. Paz, and M. Ordonez, "Improving DC microgrid dynamic performance using a fast state-plane-based source-end controller," *IEEE Trans. Power Electron.*, vol. 34, no. 8, pp. 8062–8078, Aug. 2019.

[17] D. Fulwani, S. Singh, and V. Kumar, "Robust sliding-mode control of dc/dc boost converter feeding a constant power load," *IET Power Electron.*, vol. 8, no. 7, pp. 1230–1237, Jul. 2015.

[18] L. Michel, C. Join, M. Fliess, P. Sicard, and A. Cheriti, "Model-free control of dc/dc converters," in *Proc. IEEE 12th Workshop Control Model. Power Electron.*, Boulder, CO, USA, 2010, pp. 1–8.

[19] L. Menhour, B. d'Andrea-Novel, M. Fliess, D. Gruyer, and H. Mounier, "A new model-free design for vehicle control and its validation through an advanced simulation platform," in *Proc. Eur. Control Conf.*, Linz, Austria, 2015, pp. 2114–2119.

[20] H. Abouaïssa and S. Chouraqui, "On the control of robot manipulator: A model-free approach," *J. Comput. Sci.*, vol. 31, pp. 6–16, Feb. 2019.

[21] A. H. Gomaa Haroun and Y. Li, "A novel optimized hybrid fuzzy logic intelligent PID controller for an interconnected multi-area power system with physical constraints and boiler dynamics," *ISA Trans.*, vol. 71, pp. 364–379, Nov. 2017.

[22] X. Zhang, H. Wang, Y. Tian, L. Peyrodie, and X. Wang, "Model-free based neural network control with time-delay estimation for lower extremity exoskeleton," *Neurocomputing*, vol. 272, pp. 178–188, Jan. 2018.

[23] H. P. Wang, G. I. Y. Mustafa, and Y. Tian, "Model-free fractional-order sliding mode control for an active vehicle suspension system," *Advances Eng. Softw.*, vol. 115, pp. 452–461, Jan. 2018.

[24] A. M. Bassam, A. B. Phillips, S. R. Turnock, and P. A. Wilson, "Development of a multi-scheme energy management strategy for a hybrid fuel cell driven passenger ship," *Int. J. Hydrogen Energy*, vol. 42, no. 1, pp. 623–635, Jan. 2017.

[25] A. Emadi, A. Khaligh, C. H. Rivetta, and G. A. Williamson, "Constant power loads and negative impedance instability in automotive systems: Definition, modeling, stability, and control of power electronic converters and motor drives," *IEEE Trans. Vehicular Technol.*, vol. 55, no. 4, pp. 1112–1125, Jul. 2006.

[26] D. K. Fulwani and S. Singh, *Mitigation of Negative Impedance Instabilities in DC Distribution Systems*. Singapore: Springer Singapore, 2017.

[27] M. M. Mardani, N. Vafamand, M. H. Khooban, T. Dragicevic, and F. Blaabjerg, "Design of quadratic d-stable fuzzy controller for DC microgrids with multiple CPLs," *IEEE Trans. Ind. Electron.*, vol. 66, no. 6, pp. 4805–4812, Jun. 2019.

[28] A. Sarabakha, C. Fu, E. Kayacan, and T. Kumbasar, "Type-2 Fuzzy logic controllers made even simpler: From design to deployment for UAVs," *IEEE Trans. Ind. Electron.*, vol. 65, no. 6, pp. 5069–5077, Jun. 2018.

[29] M. Mehndiratta, E. Kayacan, and T. Kumbasar, "Design and experimental validation of single input type-2 fuzzy PID controllers as applied to 3 DOF helicopter testbed," in *Proc. IEEE Int. Conf. Fuzzy Syst.*, Vancouver, BC, Canada, 2016, pp. 1584–1591.

[30] T. Kumbasar, "Robust stability analysis and systematic design of single-input interval type-2 fuzzy logic controllers," *IEEE Trans. Fuzzy Syst.*, vol. 24, no. 3, pp. 675–694, Jun. 2016.

[31] T. MohammadRidha *et al.*, "Model free iPID control for glycemia regulation of type-1 diabetes," *IEEE Trans. Biomed. Eng.*, vol. 65, no. 1, pp. 199–206, Jan. 2018.

[32] Y. A. Younes, A. Drak, H. Noura, A. Rabhi, and A. E. Hajjaji, "Robust model-free control applied to a quadrotor UAV," *J. Intell. Robot. Syst.*, vol. 84, no. 1–4, pp. 37–52, Dec. 2016.

[33] B. Ning, S. Cheng, and Y. Qin, "Direct torque control of PMSM using sliding mode backstepping control with extended state observer," *J. Vib. Control*, vol. 24, no. 4, pp. 694–707, Feb. 2018.

[34] S. Li, H. Wang, Y. Tian, A. Aitouch, and J. Klein, "Direct power control of DFIG wind turbine systems based on an intelligent proportional-integral sliding mode control," *ISA Trans.*, vol. 64, pp. 431–439, Sep. 2016.

[35] M. M. Mardani, M. H. Khooban, A. Masoudian, and T. Dragicevic, "Model predictive control of DC–DC converters to mitigate the effects of pulsed power loads in naval DC microgrids," *IEEE Trans. Ind. Electron.*, vol. 66, no. 7, pp. 5676–5685, Jul. 2019.

Mohammad Hassan Khooban (M'13–SM'18) received the Ph.D. degree in power systems and electronics from the Shiraz University of Technology, Shiraz, Iran, in 2017.

From 2016 to 2017, he was a Research Assistant with the University of Aalborg, Aalborg, Denmark, conducting research on advanced control of microgrids and marine power systems. From 2017 to 2018, he was a Postdoctoral Associate with Aalborg University. He is currently a Postdoctoral Fellow with Aarhus University, Aarhus, Denmark. He has authored or coauthored more than 130 publications on journals and international conferences, one book chapter, and holds one patent. His current research interests include control theory and application, power electronics, and its applications in power systems, industrial electronics, and renewable energy systems.

Dr. Khooban is currently the Guest Editor/Associate Editor for the Complexity Journal and the IEEE JOURNAL OF EMERGING AND SELECTED TOPICS IN POWER ELECTRONICS. He also serves extensively as a Reviewer for various IEEE/IET transactions and journals on power electronics, circuits, and control engineering.

Meysam Gheisarnejad received the B.Sc. degree in electronic engineering from Azad University, Lahijan, Iran, in 2009 and the M.Sc. degree in control engineering from Azad University, Najafabad, Iran, in 2013.

His research interests include power system dynamics and control, shipboard microgrid, cyber-physical microgrid, power electronics, and renewable energy systems.

Hamed Farsizadeh was born in Shiraz, Fars, Iran. He received the B.Sc. degree in electrical engineering from Fars Science and Research Branch (FSRIAU) in 2009. He is currently working toward the M.Sc. degree in power electronics with the Shiraz University of Technology, Shiraz, Iran.

His main research interests include power elecronic, control of modern power grids, and advanced control of dc–dc power converters.

Ali Masoudian was born in Kazeroon, Fars, Iran, in 1987. He received the M.S. degree in power engineering in 2013 from Shiraz University, Shiraz, Fars, Iran, where he is currently working toward the Ph.D. degree.

He is currently with the Moheb Nirou consulting company, Shiraz, Fars, Iran, as the Head of Power System Studies and Planning Group. His research interests include power electronics, power system optimization and planning, microgrid design and management, shipboard power systems, and electric vehicles control systems.

Jalil Boudjadar (M'18) received the Ph.D. degree from Toulouse University, France, in Dec. 2012.

He is currently an Assistant Professor with the Department of Engineering, Aarhus University, Aarhus, Denmark. He is also a member of the DIGIT Research Centre. Before joining Aarhus University, he did research for 4 years at different prestigious universities in Canada and Sweden. He is currently doing intensive research on energy-related performance and safety control for shipboard systems. His research interests include the design, safety, and performance of embedded systems and control.